Cross-scale excitability in networks of quadratic integrate-and-fire neurons

Daniele Avitabile, Mathieu Desroches, G Bard Ermentrout

CROSS-SCALE EXCITABILITY IN NETWORKS OF QUADRATIC INTEGRATE-AND-FIRE NEURONS.

DANIELE AVITABILE*, MATHIEU DESROCHES†, AND G. BARD ERMENTROUT‡

Abstract. From the action potentials of neurons and cardiac cells to the amplification of calcium signals in oocytes, excitability is a hallmark of many biological signalling processes. In recent years, excitability in single cells has been related to multiple-timescale dynamics through *canards*, special solutions which determine the effective thresholds of the all-or-none responses. However, the emergence of excitability in large populations remains an open problem. Here, we show that the mechanisms of excitability in an infinite heterogeneous population of coupled quadratic integrate and fire (QIF) cells maintains echoes of the mechanism for the individual components. We exploit the Ott-Antonsen ansatz to derive low-dimensional dynamics for the coupled network and use it to describe the structure of canards via slow periodic forcing. We demonstrate that the thresholds for onset and offset of population firing can be found in the same way as those of the single cell. We combine theoretical and numerical analysis to develop a novel and comprehensive framework for excitability in large populations.

Key words. slow-fast dynamics, bursting, mean-field limit, Ott-Antonsen ansatz, QIF neurons, canards

1. Introduction.

Excitability is a fundamental *all-or-none* property of many living cells including neurons [1]. It manifests itself by a very nonlinear response to a sufficiently strong external input leading to the emission an action potential before going back to a rest state, whereas any weaker input has no effect on the cell other than a small fluctuation of the membrane potential around its equilibrium value. The concept of excitability is well known to biologists, in particular through the existence of a non-observable boundary in the response space marking the abrupt transition from rest to spike. However, while the geometry of single-cell excitability is well understood [20], the idea of population excitability (for example in a network of coupled neurons) has been far less studied. What makes a population respond normally (such as in working memory tasks [3]) or abnormally (such as in seizures and other pathologies [12]) is a critical question in neuroscience.

Most biophysical and phenomenological models of class II membranes [10] — Hodgkin-Huxley (HH), FitzHugh-Nagumo (FHN), Morris-Lecar (ML)— share similar geometrical features and their excitability threshold is shaped through the intrinsic slow-fast dynamics of these models. In particular, in planar models of HH, FHN or ML type, and some three-dimensional ones, the best approximation of the excitability threshold is given by so-called *canard solutions* [5, 15, 23], which follow the repelling middle branch of the cubic nullcline (nullsurface in 3D) of the model. In single cells, canard solutions underpin complex biological rhythms [22], organise transitions from resting to spiking states [16], and from spiking to bursting regimes [13].

The canonical class I excitable systems such as the QIF neuron models, and equivalently the theta-neuron models [9], do not intrinsically possess multiple timescales. Nevertheless slow periodic forcing can bring out a bursting rhythm in theta neurons and the threshold to bursting dynamics is again formed by canard solutions [6]. Networks of QIF neurons are capable of generating similar bursting rhythms upon

*Department of Mathematics, Vrije Universiteit Amsterdam, Netherlands (d.avitabile@vu.nl).
†MathNeuro Team, Inria Sophia Antipolis Méditerranée, France (mathieu.desroches@inria.fr).
‡Department of Mathematics, University of Pittsburgh, Pittsburgh, USA (bard@pitt.edu).

[1] For simplicity, we describe neuronal excitability, but this notion extends beyond membrane biophysics.

periodic input [17, 21], so the question of network excitability and threshold comes naturally in this context.

In this work, we provide a novel approach to the question of population excitability by showing that the geometry of excitability at the microscopic level scales up to large networks, involving similar key objects related to the slow-fast nature of the system. We build on the results by Ott and Antonsen [18] in the case of dense (all-to-all) networks of QIF neurons, with randomly distributed constant inputs following a heavy-tail (Lorentzian) distribution. For this network there exists a simple mean-field limit, namely an ODE [4, 8, 14, 19]. We show that excitability in large networks of this type is organised via canards in the very same way that it is at the mean-field limit, and we showcase these results computationally by exhibiting an accurate approximation of the network threshold for networks of size $N = 10^5$. Thus, the geometry of excitability in QIF neural networks beautifully persists across scales. However, for large-enough networks (and up to the mean-field limit) it only reveals itself once we consider the correct macroscopic variables, namely the firing rate and the mean membrane potential. This is in contrast to the single-neuron level where there is no rate and hence the slow-fast variables endowed with this excitable geometry only encompass the membrane potential.

Our results reveal that canards form an interface for excitable transitions, from *down network states* (neural population silent phase) up to *network bursting* —as observed in [17] but without explanation of the threshold transition— as well as for the dual transitions from *up network states* (neural population tonic firing) down to *network bursting* which was not reported before and involves the same canard geometry and dynamics.

2. QIF Network model. We study a network of N all-to-all coupled QIF neurons. The ith neuron is characterised by the membrane potential V_i, the synaptic variable s_i, and is subject to both a background current η_i, and an external, zero-mean current $I(t) = A\sin(\varepsilon t)$, leading to the following evolution equations, for $1 \leqslant i \leqslant N$,

$$V_i' = V_i^2 + \eta_i + I(t) + \frac{J}{N}\sum_{j=1}^{N} s_j, \qquad s_i' = -s_i/\tau_s. \tag{2.1}$$

We refer to the sum $K_i = \eta_i + I(t)$, as the external input (or simply *input*) to the ith cell. The ODEs above hold between two consecutive firing times: these are the finite, computable times at which a membrane potential in the network diverges to $+\infty$ [2]. Each time this condition is met by V_i we: (i) stop the simulation, (ii) reset V_i to $-\infty$, (iii) send a spike to *all synapses*, whose values are instantaneously incremented by an amount $1/N$; (iv) restart the simulation of (2.1) from these updated initial conditions. This system is ideally suited to study excitability across scales because: (i) we can analyse and compare single cell-dynamics, $N = 1$, network dynamics $N \gg 1$, and mean-field dynamics $N \to \infty$; (ii) one can switch from constant input currents ($\varepsilon = 0$) to slowly-varying, oscillatory currents ($0 < \varepsilon \ll 1$) in order to uncover transitions between various cellular regimes.

2.1. Single-neuron excitability. Let us set $N = 1$, $\varepsilon = 0$, and examine a QIF neuron with self-coupled synapse [2], subject to a constant input current $K_1 = \eta_1$ (see Figure 1(a,b)). When $0 < \tau_s \ll 1$ and $J\tau_s$ is sufficiently large, the cell supports

[2] Using the transformation $V_i = \tan\theta_i/2$, one arrives at $\theta_i' = 1 - \cos\theta_i + (1+\cos\theta_i)\big[I(t) + \eta_i + \frac{J}{N}\sum_{j=1}^{N} s_j\big]$, $s_i' = -s_i/\tau_s$, and computes a firing event when θ_i crosses the value $\pi/2$ from below.

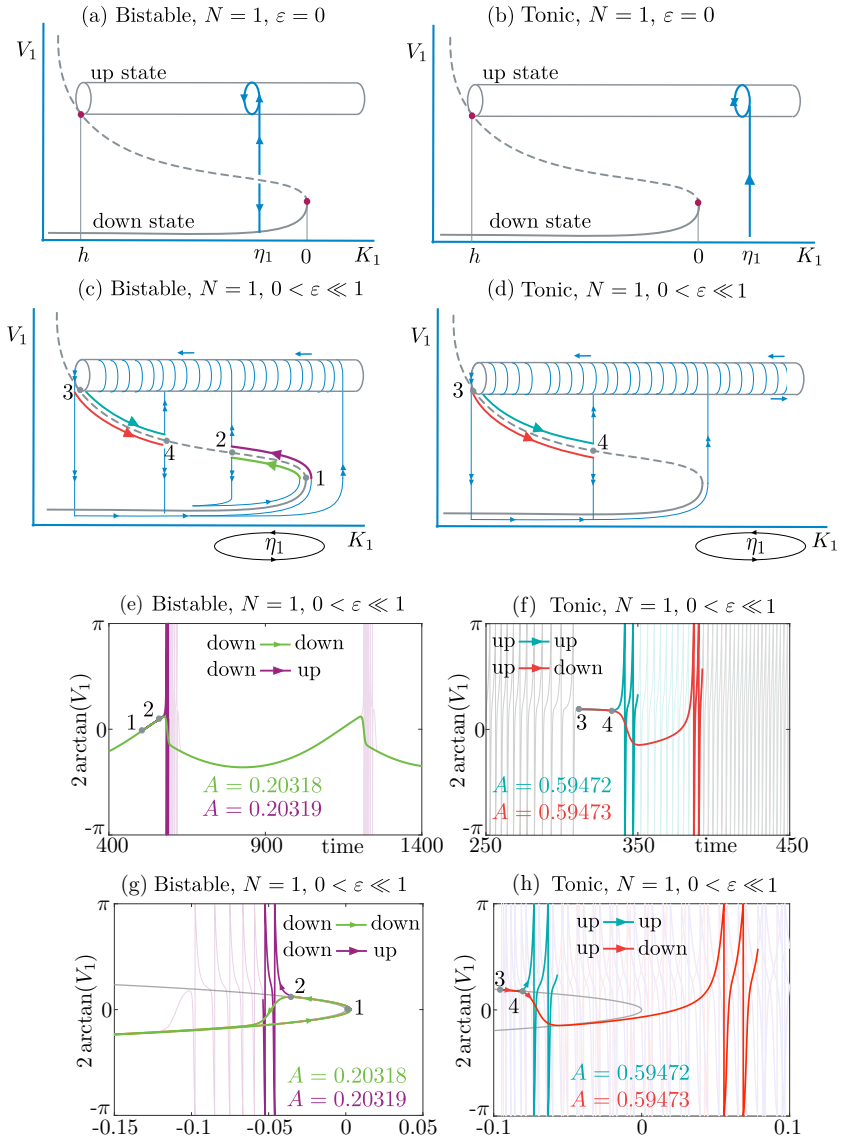

FIG. 1. *(a,b): Sketch (not to scale) of the bifurcation diagram of steady states (curve) and periodic solutions (cylinder) of a single QIF neuron ($N = 1$ in Eq. (2.1)) subject to a constant input $K_1 = \eta_1$ ($\varepsilon = 0$). A stable quiescent state (down state) coexists with a stable tonic firing solution (up state), separated by an unstable equilibrium (dashed curve). A homoclinic bifurcation is present when $K_1 = h$. An intrinsically bistable cell ((a), $K_1 = \eta_1 \in (h, 0)$), selects the up or down state depending on initial conditions. An intrinsically tonic cell ((b), $K_1 = \eta_1 > 0$) displays solely the firing solution (up state). (c,d): When $0 < \varepsilon \ll 1$, $K_1(t) = \eta_1 + A\sin(\varepsilon t)$ becomes a slowly varying quantity, oscillating around the value of η_1 (ellipses on the K_1 axes), and transitions between the up and the down phases become possible. (c): The onset between phases is determined by a continuum of special solutions, that follow for some time the unstable middle state (canard solutions); in the bistable regime they appear in the down-down (green), down-up (purple), up-down (red), and up-up (cyan) transitions. (d): When $K_1(t)$ oscillates around a tonic value $\eta_1 > 0$, canards are possible as up-up and up-down transitions, but not vice-versa. (e): Time profiles of two solutions, in the bistable regime with slow input $K_1(t)$, displaying a down-down and down-up transition, containing a canard segment (1–2). (f): Time profiles of two solutions in the tonic regime, with slow input $K_1(t)$, displaying an up-up and up-down transition, containing a canard segment (3–4). (g,h): The solutions in (e,f) are plotted in the variables (V_1, K_1), and superimposed on the curve of equilibria of the $\varepsilon = 0$ system (grey parabola), providing evidence of the scenarios sketched in (c,d), with canards labeled 1–2 and 3–4 in all diagrams, and part of the orbits greyed out to enhance visibility. Parameters in (e,g): $\varepsilon = 0.01$, $J = 6$, $\tau_s = 0.3$, $\eta_1 = -0.2$, $A = 0.20318$ (down-down) and $A = 0.20319$ (down-up). Parameters in (f,h): $\varepsilon = 0.01$ $J = 6$, $\tau_s = 0.3$ $\eta_1 = 0.5$, $A = 0.59472$ (up-up) and $A = 0.59473$ (up-down).*

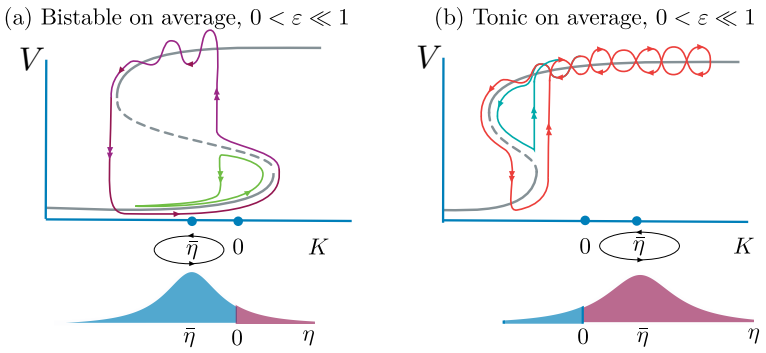

FIG. 2. *Network where the currents η_i are randomly distributed (bottom panels), hence some neurons are bistable (blue) and others are tonic (red), with average $\overline{\eta}$. The $\varepsilon = 0$ equilibria lie on S-shaped curve (grey). The up state is no longer a periodic orbit as in Figure 1, but a high-voltage, high-rate equilibrium. The geometry of excitability, however, persists when $\varepsilon \ll 1$, and $K(t)$ oscillates slowly around $\overline{\eta}$. We sketch examples of down-down, and down-up transitions when the distribution is bistable on average ((a), $\overline{\eta} < 0$), and of up-up and up-down transitions when the distribution is tonic on average ((b), $\overline{\eta} > 0$). When $A \gg \overline{\eta}$ synchronous firing occurs near the upper branch of the S-shaped curve.*

two characteristic *coexisting attracting* states: an equilibrium (*down state*), and a periodic solution with tonic firing (*up state*), separated by an intermediate unstable equilibrium. The equilibria belong to a curve which folds when the input is null; periodic solutions collide with unstable equilibria at a homoclinic bifurcation, when the input equals h.

For $\varepsilon = 0$ and $\eta_1 \in (h, 0)$ in (2.1) (intrinsically bistable regime), the initial conditions determine whether the voltage is attracted to the down state, or to the up state (Figure 1(a)); the threshold is given by the middle unstable state. When $\eta_1 > 0$, the only attractor is the periodic solution, hence the cell is intrinsically tonic (Figure 1(b)). We are interested in how the cell (and later on, the network) transitions from the rest state to the repetitive firing state, and how the two states are concatenated together to form a bursting state. In a standard QIF model without synapses ($J = 0$), there is no bistability (the up state is to the right of the fold): this changes some of the waveforms supported by the cell, but not the mechanisms we aim to describe, namely the bursting transitions between down and up states [6].

To study these transitions, one sets $\varepsilon > 0$ small and hence examines slow forcing [10,20], as sketched in Figure 1(c,d). This causes the input to oscillate around the mean value η_1, as represented by the small ellipses on the horizontal axes. The exact dynamics of the system depends on A, the amplitude of the input oscillations, and one can construct a great variety of solutions where up and down states alternate. Some trajectories stand out, in that they signal the onset or termination of a phase. With reference to Figure 1(c), small-amplitude forcing with average $\eta_1 \in (h, 0)$ causes the cell to oscillate around its rest state; these are subthreshold oscillations, which stick to the down state at all times; a temporal profile of this solution is given in Figure 1(e) obtained for $A = 0.20318$, $\varepsilon = 0.01$ (green). Upon increasing A to 0.20319, we find a bursting state (purple curve). This remarkably sharp transition is determined by a *continuum of solutions*, which follow the branch of unstable states for increasingly longer times (segments 1–2), before jumping to the down state, or to the up state. These counter-intuitive orbits contain canard segments (marked with colors and numbers in panel (c)), occur in a narrow region of parameters, and form a computable

interface between subthreshold oscillations (down-down orbits) and bursting states (down-up orbits). Canard orbits are also present in the transition from modulated spiking to bursting states (up-up and up-down orbits, segments 3–4 in Figure 1(c)). If a cell is intrinsically tonic we find up-up and up-down orbits with canards Figure 1(d,f,h), whereas it is possible to prove that down-down and down-up canards cannot exist, that is, the transition at the fold is a jump. The orbits described above capture excitability transitions at a single-cell level.

2.2. Network Excitability. Having reviewed single-cell excitability, we turn to network excitability. We consider the network (2.1), together with reset conditions, subject to random background currents: η_i are taken from the Lorentzian distribution with density $g(\eta) = \Delta/(\pi(\eta - \bar{\eta})^2 + \pi\Delta^2)$, hence the network is heterogeneous, with some neurons in the bistable regimes, and others in the tonic regime. However, the network average will turn out to play a role: if $\bar{\eta} < 0$ ($\bar{\eta} > 0$) the distribution is said to be bistable (tonic) on average. For $N \to \infty$, there is a well-known mean-field limit [7, 17] for the coupled system:

$$\begin{aligned} r' &= \Delta/\pi + 2rv, \\ v' &= v^2 - \pi r^2 + Js + \bar{\eta} + I(t), \\ s' &= (-s + r)/\tau_s, \end{aligned} \tag{2.2}$$

where r, v, s are the mean firing rate, mean membrane potential, and mean synaptic current, respectively. It is important to remark that the mean-field limit introduces a new quantity, the population firing rate, r [7] that is not a part of the single or finite system of equations. It emerges in the limit as $N \to \infty$ of the microscopic model (2.1). As seen in Figure 2, when $\varepsilon = 0$, hence $K(t) \equiv \overline{\eta}$, the equilibria of the system lie on an S-shaped curve. The down state is a configuration in which all neurons are close to rest (quiescent network state), whereas the up state corresponds to asynchronous network tonic firing (an averaged version of the tonic state in Figure 1). The up state can be a stable focus away from the fold and have complex eigenvalues. Between these two stable fixed points is an unstable (saddle) point that serves as a separatrix between the two stable states. Remarkably, when $0 < \varepsilon \ll 1$, the geometry of excitability still persists in this macroscopic description, and transitions are now determined by the average $\overline{\eta}$ of the distributions. We now show that the transitions of the mean field and of the network directly parallel the transitions of the single neuron model, involving the same canard types.

2.2.1. QIF network with bistable average. In Fig. 3(b) we show a simulation with $\varepsilon = 0.05$, $\bar{\eta} = -15.1$ for two different values of the maximum amplitude of the stimulus, A, superimposed on the S-shaped curve of equilibrium for $\varepsilon = 0$ (grey). One trajectory (green) follows the down state, along the bottom branch. The trajectory hugs the unstable branch of fixed points (the canard segment) past the fold F^-, and then jumps down. Small changes in A result in a divergence from the down-down (green) to the down-up (purple) states. By varying continuously A one can find a trajectory that follows the unstable branch up to F^+ (not shown). This trajectory acts as an *excitability threshold*, separating down-down from down-up orbits.

The qualitative difference between the two behaviors is more striking in the time traces of the two curves, shown in Fig. 3(a), where the transition to the up state is accompanied by a burst while for the smaller input, there is just a subthreshold oscillation. The reason for the burst is that the up state is a stable spiral for a range of input values. We will later show that this transition is determined by a folded-saddle

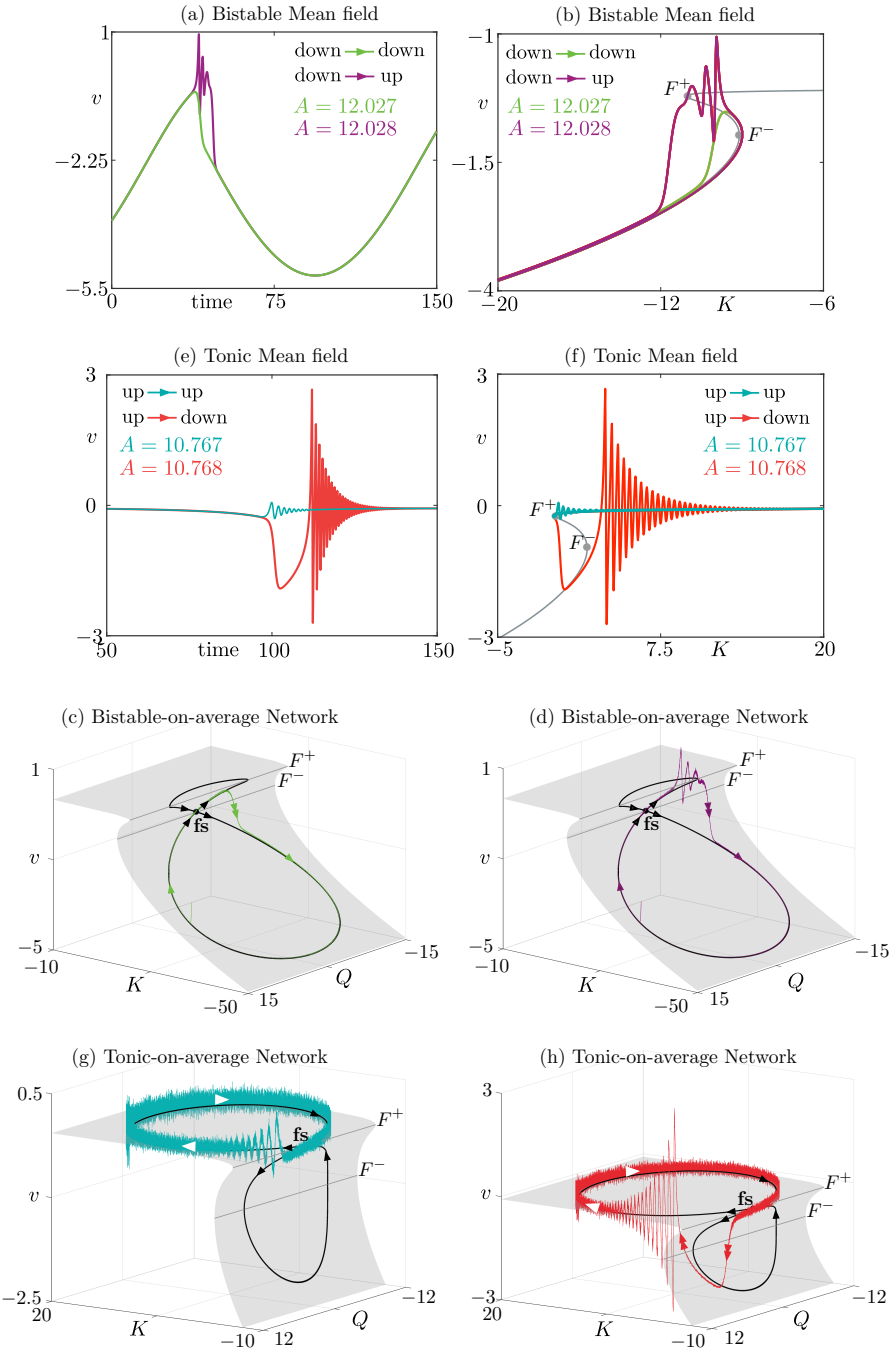

FIG. 3. *Mean field (2.2) (a,b,e,f) vs Network (2.1) with $N = 10^5$ neurons (c,d,g,h) when the input is slowly varying. Parameters are $\Delta = 1$, $J = 15$, $\tau = 0.002$, $\varepsilon = 0.05$. Top (bottom) panels show the bistable (tonic) regime, reaching population bursting via two canard scenarios, down-up and up-down, respectively. In each row, panels display (left to right) mean-field v time profile of both solutions, their (K, v) projection as in Fig. 1(g,h), and two corresponding network solutions shown separately in 3D phase space (K, Q, v), where $Q = I'$, together with the (grey) surface of equilibria when $\varepsilon = 0$, folded along the two lines $F^{\pm}$ (also shown in (b,f)). Key to threshold dynamics is the folded saddle (fs) and its associated canards (black curves), which shape the behaviour of trajectories across this transition. The network simulation mirrors the mean field prediction (black lines) (a,b): $\overline{\eta} = -15.1$, $A = 12.027$ (down-down), $A = 12.028$ (down-up);(e,f): $\overline{\eta} = 5$, $A = 10.767$ (up-up), $A = 10.768$ (up-down).*

canard, just as it was in the single neuron case. When $A \gg \bar{\eta}$ the network transitions smoothly (without canards) from asynchronous to synchronous firing, following the upper branch of the S-shaped curve in Figures 2 and 3.

2.2.2. QIF network with tonic average. In Fig. 3(f) we have set $\bar{\eta} = 5$ and so the only possible behavior without forcing is tonic firing (recall the rotating symbols in Figure 2(b)). A similar situation occurs as in the excitable case, but the dynamics revolves around the upper fold F^+, and a canard is now associated with a different route to bursting, separating the up-up from the up-down scenarios. As with the excitable case, the differences are more evident when we plot the mean voltage as a function of time, in Figure 3(e). The mechanism for excitability here is also a folded-saddle canard as we will now discuss.

2.2.3. Folded-saddle canard behavior across scales. We now derive two central results of the paper: firstly, we characterise the mean-field transitions described above, valid at ODE level (system (2.2)), using standard methods from Geometric Singular Perturbation Theory [11]; secondly, we use this characterisation to infer the existence of a canard behavior at network level (system (2.1)) with $N = 10^5$ neurons, and provide numerical evidence of this phenomenon. The latter result is remarkable and novel, as canard behavior in large networks is greatly unexplored, in particular for systems with resets and random data.

To study the behavior of Eq. (2.2) for small $\varepsilon > 0$, we extend the system with two ODEs describing the oscillatory dynamics of $K(t)$, namely $K' = \varepsilon Q$, $Q' = -\varepsilon(K - \bar{\eta})$. We then rescale time by $\tau = t/\varepsilon$, set $\varepsilon = 0$, and obtain $r = s = -\Delta/(2\pi v)$, hence

$$0 = K + \psi(v), \quad \dot{K} = Q, \quad \dot{Q} = -(K - \bar{\eta}), \tag{2.3}$$

where $\psi(v) = v^2 - \Delta^2/(4\pi v^2) - J\Delta/(2\pi v)$. Differentiating with respect to τ (overdot), the first equation gives

$$-D\psi(v)\dot{v} = Q, \qquad \dot{Q} = \psi(v) + \bar{\eta},$$

which is a singular system when the derivative $D\psi$ is null, that is, at the folds $F^{\pm}$ in Fig. 3. A further time rescaling, using the nonlinear transformation $\tau \mapsto -D\psi(v)\tau$, yields the desingularised system:

$$\dot{v} = Q, \quad \dot{Q} = -D\psi(v)\big(\psi(v) + \bar{\eta}\big). \tag{2.4}$$

An equilibrium $(v_*, 0)$ of (2.4) satisfying $D\psi(v_*) = 0$ is called a *folded singularity*, whose classification gives insight into how trajectories of system (2.2) with small $\varepsilon > 0$ cross the fold. Since $\psi(v)$ is cubic-like, there are two roots corresponding to the folds, $F^{\pm}$ in Fig. 3 and a linearization of Eq. (2.4) reveals that they are both saddle points (*folded saddles* in the original system (2.2)). For the excitable (tonic) case, the relevant saddle is the one at F^- (F^+). As Eq. (2.4) is an integrable system, the stable and unstable manifolds of these saddles form closed orbits (homoclinic connections) that are the basis for the canards observed in Fig. 3.

Fig. 3(c,d,g,h) display the dynamics of Eq. (2.4) (in black) superimposed on the dynamics of Eq. (2.1) with $N = 10^5$ (in color), for sub and suprathreshold forcing. The black curves form a pair of homoclinic loops intersecting on F^- at the folded saddle (fs), and represent the dynamics for the $\varepsilon = 0$ limit. Fig. 3(c) shows, in green, the *full network orbit with* $N = 10^5$ for A slightly smaller than the threshold. A canard segment is visible, where the trajectory hugs the black curve on the fold before falling

back to the down state. Fig. 3(d) shows the same projection, but for slightly larger A; in this case, the trajectory makes the jump to the up state before falling back down. The folded-saddle canards predicted by mean-field theory (in black) are in striking agreement with the behaviour of the network, and the similarity with the mean-field transitions in 3(b) is remarkable. These are analogues of the down-down and down-up scenarios for the single neuron model, but they are exhibited at the level of the network.

Fig. 3(g,h) show the dynamics of Eq. (2.4) (black) and Eq. (2.1) with $N = 10^5$ (in color) in the tonic case. As we saw in Fig. 3(e,f), the canard appears across the upper fold, F^+ and the up-up transition appears when A exceeds the threshold of roughly 10.76. As with the excitable case, a folded-saddle canard behaviour explains the transition between up-up (asynchronous) and up-down (bursting) network states.

3. Conclusion. The geometry of excitability and transition to bursting behavior in single neurons and allied systems is governed by canard solutions, which act as thresholds and determine the response of the system to slow parametric changes. We have shown that this structure carries over in the mean-field limit of large populations of excitable cells, as well as in large finite systems. In these cases the average voltage of the population plays the same role as the voltage in the single cell and the mean input determines whether the population behaves as a forced excitable or intrinsically oscillatory medium. We expect that similar properties will survive in networks of more realistic cells, up to their mean field-limit, which need not be an ODE. Introduction of inhibitory networks could provide a connection between this work and the concept of balanced networks where, depending on the details of the connection strengths, the firing is either driven by the mean input (analogous to our tonic behavior) or by the fluctuations (analogous to the excitable case). There is currently no available theory for such cases, except for continuous coarse-grained networks [1], but a numerical exploration of the averaged voltages and synaptic variables may reveal an underlying low-dimensional structure, similarly to what has been found in spatially-extended neural field models.

REFERENCES

[1] D. Avitabile, M. Desroches, and E. Knobloch, *Spatiotemporal canards in neural field equations*, Phys. Rev. E, 95 (2017), p. 042205.
[2] C. Börgers, R. M. Takeuchi, and D. T. Rosebrock, *On rhythms in neuronal networks with recurrent excitation*, Neural Comput., 30 (2018), pp. 333–377.
[3] A. Compte, N. Brunel, P. S. Goldman-Rakic, and X.-J. Wang, *Synaptic mechanisms and network dynamics underlying spatial working memory in a cortical network model*, Cereb. Cortex, 10 (2000), pp. 910–923.
[4] S. Coombes and A. Byrne, *Next generation neural mass models*, in Nonlinear Dynamics in Computational Neuroscience, Springer, 2019, pp. 1–16.
[5] M. Desroches, M. Krupa, and S. Rodrigues, *Inflection, canards and excitability threshold in neuronal models*, J. Math. Biol., 67 (2013), pp. 989–1017.
[6] M. Desroches, M. Krupa, and S. Rodrigues, *Spike-adding in parabolic bursters: The role of folded-saddle canards*, Phys. D, 331 (2016), pp. 58–70.
[7] F. Devalle, A. Roxin, and E. Montbrió, *Firing rate equations require a spike synchrony mechanism to correctly describe fast oscillations in inhibitory networks*, PLoS Comput. Biol., 13 (2017), p. e1005881.
[8] M. di Volo and A. Torcini, *Transition from asynchronous to oscillatory dynamics in balanced spiking networks with instantaneous synapses*, Phys. Rev. Lett., 121 (2018), p. 128301.
[9] G. B. Ermentrout and N. Kopell, *Parabolic bursting in an excitable system coupled with a slow oscillation*, SIAM J. Appl. Math., 46 (1986), pp. 233–253.
[10] E. M. Izhikevich, *Dynamical systems in neuroscience*, MIT press, 2007.

[11] C. K. R. T. Jones, *Geometric singular perturbation theory*, in Dynamical Systems, vol. 1609 of Lect. Notes Math., Springer-Verlag, 1995, pp. 44–118.
[12] M. A. Kramer et al., *Human seizures self-terminate across spatial scales via a critical transition*, Proc. Natl. Acad. Sci. USA, 109 (2012), pp. 21116–21121.
[13] M. A. Kramer, R. D. Traub, and N. J. Kopell, *New dynamics in cerebellar purkinje cells: torus canards*, Phys. Rev. Lett., 101 (2008), p. 68103.
[14] C. R. Laing, *Exact neural fields incorporating gap junctions*, SIAM J. Appl. Dyn Syst., 14 (2015), pp. 1899–1929.
[15] J. Mitry, M. McCarthy, N. Kopell, and M. Wechselberger, *Excitable neurons, firing threshold manifolds and canards*, J. Math. Neurosci., 3 (2013), pp. 1–32.
[16] J. Moehlis, *Canards for a reduction of the hodgkin-huxley equations*, J. Math. Biol., 52 (2006), pp. 141–153.
[17] E. Montbrió, D. Pazó, and A. Roxin, *Macroscopic description for networks of spiking neurons*, Phys. Rev. X, 5 (2015), p. 021028.
[18] E. Ott and T. M. Antonsen, *Macroscopic description for networks of spiking neurons*, Chaos, 18 (2008), p. 037113.
[19] B. Pietras, F. Devalle, A. Roxin, A. Daffertshofer, and E. Montbrió, *Exact firing rate model reveals the differential effects of chemical versus electrical synapses in spiking networks*, Phys. Rev. E, 100 (2019), p. 042412.
[20] J. Rinzel and G. B. Ermentrout, *Analysis of neural excitability and oscillations*, in Methods in neuronal modeling: From synapses to networks, 2nd ed., C. Koch and I. Segev, eds., Cambridge (MA), USA, 1988, MIT Press, pp. 251–291.
[21] H. Schmidt, D. Avitabile, E. Montbrió, and A. Roxin, *Network mechanisms underlying the role of oscillations in cognitive tasks*, PLoS Comput. Biol., 14 (2018), p. e1006430.
[22] T. Vo, M. A. Kramer, and T. J. Kaper, *Amplitude-modulated bursting: A novel class of bursting rhythms*, Phys. Rev. Lett., 117 (2016), p. 268101.
[23] M. Wechselberger, J. Mitry, and J. Rinzel, *Canard theory and excitability*, in Nonautonomous dynamical systems in the life sciences, vol. **2102** of Lect. Notes Math., Springer, 2013, pp. 89–132.